AIAA JOURNAL
Vol. 44, No. 10, October 2006

Flutter Characteristics of Reentry Space Vehicle with Nonplanar Wing

Atsushi Kanda*
Japan Aerospace Exploration Agency, Mitaka, Tokyo 181-0015, Japan
Tetsuhiko Ueda†
Nagoya University, Nagoya, Aichi 464-8603, Japan
and
Takashi Kai‡
Japan Aerospace Exploration Agency, Mitaka, Tokyo 181-0015, Japan

DOI: 10.2514/1.18444

A reentry space vehicle with nonplanar wings, which was planned to be developed in Japan, has a roll elastic freedom during launch. This is because of an attachment between the vehicle and the launch rocket. This study describes the flutter characteristics of a reentry space vehicle model in both launching and free-flight configurations. Results of wind tunnel tests and analyses reveal that the antisymmetric mode flutter becomes critical in both configurations and the existence of the roll elastic freedom further decreases the critical flutter speed. The result also shows that the analytical and experimental flutter speeds differ significantly in the supersonic region. Corrected analysis is conducted by using the measured local Mach number, and it is found that the interference between the blunt fuselage and nonplanar wings results in a discrepancy in the flutter speed.

Nomenclature

b	=	half chord length at root
f_α	=	natural frequency of first torsion mode
M	=	Mach number
M_1	=	local Mach number
M'	=	corrected Mach number
m	=	wing mass
P	=	static pressure
P_1	=	static pressure in local flow
P_2	=	static pressure behind shock wave
P_0	=	total pressure
P_{01}	=	total pressure in local flow
P_{02}	=	total pressure behind shock wave
S_w	=	wing area
U_F	=	flutter speed
$\bar{U}_F$	=	nondimensional flutter speed
γ	=	specific heat ratio
μ	=	mass ratio, $2m/(\pi\rho b S_w)$
ρ	=	air density
ω_α	=	circular frequency of first torsion mode

Introduction

THE H-II orbiting plane (HOPE) project [1,2] was initiated in Japan; currently, however, this project has been discontinued. The objective of this project is to develop a reentry space vehicle, HOPE, (Fig. 1) for transporting supplies between the International Space Station (ISS) and the Earth. It is proposed that HOPE be installed with nonplanar wings termed "tip-fins." A tip-fin wing is relatively larger than the wing fin of conventional aircraft because it performs the function of a vertical fin. The advantage of the tip-fin over a vertical fin is that it provides better control performance in the hypersonic region. Moreover, a vertical tail wing may obstruct the loading and unloading of supplies. In the flight configuration, HOPE is attached to the top of the H-IIA, an original Japanese rocket, as shown in Fig. 2 and is subsequently launched (launching configuration) and returned to the Earth (free-flight configuration).

Flutter characteristics are apparently crucial for the design of a reentry space vehicle. In the free-flight configuration, HOPE has elastic wing modes and rigid-body modes in roll, pitch, and plunge motion, as in the case of conventional aircraft. However, the design of HOPE requires special consideration in the launching configuration because HOPE has a roll elastic body mode due to an elastic attachment between the vehicle and the launch rocket. It is significantly different from conventional aircraft. The effect of the roll elastic body mode on the flutter characteristics should be examined for the launching configuration.

Flutter that is affected by a body degree of freedom is not a newly discovered phenomenon and is well known as termed "body-freedom flutter" [3,4]. Generally, the body-freedom flutter means a coupling between an elastic mode and a rigid-body mode like short-period mode [5]. A coupling between a wing bending mode and a rigid-body roll mode was shown by Weisshaar and Crittenden [6]. A wing bending mode and a rigid-body short-period mode coupling of forward-swept wings in free-free dynamic analysis was shown by Miller et al. [7], Weisshaar and Zeiler [8], and Chipman et al. [9] Body-freedom flutter of tailless aircraft (sailplanes) was showed by Banerjee [10]. Chen and Dugundji [11] conducted wind tunnel tests of body-freedom flutter of composite forward-swept wings with rigid-body pitch and plunge freedoms. The relation between body-freedom flutter speeds and supporting conditions was studied. Soistmann and Spain [12] showed body-freedom flutter of a lifting body airplane. Wu and Yang [13] showed body-freedom flutter of an airplane with high aspect ratio wings by a numerical analysis. A considerable number of studies of body-freedom flutter have been conducted as given in the preceding references. On the other hand, there are not so many studies of flutter that are affected by elastic body-freedoms. Wykes and Lawrence [14] showed a short-period structural mode coupling of a canard-delta supersonic transport. This coupling was resulting from a longitudinal short-period motion and a

Received 28 June 2005; revision received 24 March 2006; accepted for publication 25 March 2006.

*Associate Senior Researcher, Operation and Safety Technology Team, Aviation Program Group. Senior Member AIAA.
†Professor, Aerospace Engineering Department, Graduate School of Engineering. Associate Fellow AIAA.
‡Senior Researcher, Structure Technology Center, Institute of Aerospace Technology. Senior Member AIAA.

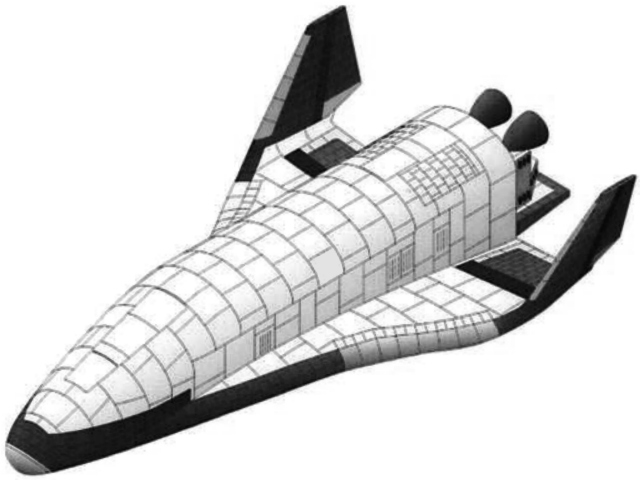

Fig. 1 HOPE.

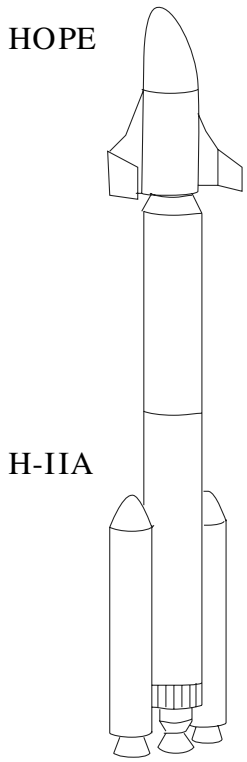

Fig. 2 Launching configuration of HOPE.

fuselage bending. Kobayashi et al. [15] studied flutter of a space plane with an elastic slender body and planar wings. A coupling between a body bending and a pitching mode was shown. Kanda et al. [16–18] studied the effects of elastic body of a space reentry vehicle in pitch and yaw motion on flutter. These studies have focused on fuselage bending in pitch or yaw only. The purpose of the present paper is to investigate flutter that is affected by a roll elastic body-freedom. The flutter characteristics of a reentry space vehicle model with a roll elastic body in the launching is estimated by wind tunnel experiments and numerical analyses using the doublet-point method (DPM) [19] for unsteady aerodynamic calculations.

Flutter in Free-Flight Configuration

This section describes the flutter characteristics of the reentry space vehicle model in the free-flight configuration. To implement this configuration in a wind tunnel test, a particular supporting system was developed. Further, a roll degree of freedom can be provided to the wind tunnel model. A flutter experiment was

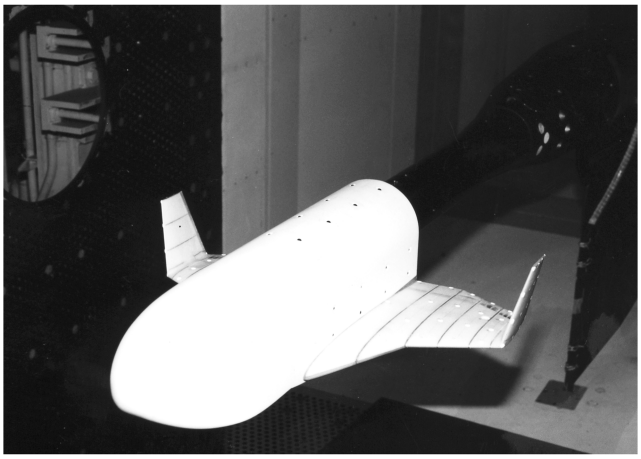

Fig. 3 Wind tunnel model for free-flight configuration.

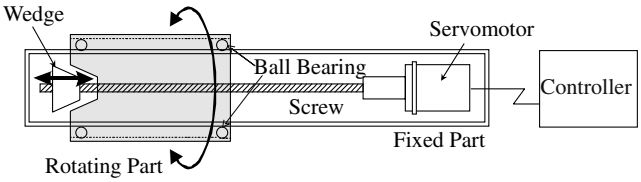

Fig. 4 Schematic of supporting system for free-flight configuration.

conducted in the 2×2 m transonic wind tunnel of the Japan Aerospace Exploration Agency (JAXA). Flutter analysis was subsequently performed by employing the DPM and the analytical and experimental results were compared.

Wind Tunnel Model and Supporting System

The wind tunnel model of the reentry space vehicle is shown in Fig. 3. The wing of the model exhibits a tip-fin configuration similar to that of HOPE and consists of a main part and the tip-fin. The wing is made of aluminum alloy 7075-T651 and covered with foam plastic to produce the shape of a NACA 0010 airfoil. Strain gauges are installed on the root of the right and left wings to measure the bending and torsion strain during the wind tunnel test. The span length of the main part is 200 mm and its chord lengths at the root and tip are 400 and 120 mm, respectively. Kinks are formed at the leading and trailing edges at a span length of 80 mm. The cant angle of the tip-fin is 14 deg and its span length is 120 mm with a chord length of 60 mm at the tip. The weight of the wing is 1.3 kg. The fuselage of the model is 677 mm in length and 160 mm in width and height.

Next, we describe the supporting system for the wind tunnel model. In the free-flight configuration, the reentry space vehicle has a roll degree of freedom. To simulate this configuration in the wind tunnel test, the supporting system has been developed and a roll degree of freedom can be provided to the wind tunnel model. Figure 4 shows the schematic of the supporting system. It is a cylindrical sting-type system composed of fixed and rotating parts. The rotating part can rotate on the cylindrical sting due to bearings. The wind tunnel model is attached to the rotating part and can have a roll degree of freedom. In addition, the supporting system can suppress flutter. The position of the wedge shown in the figure can be controlled externally. By moving the wedge rightward along the axis of the fixed part, a roll degree of freedom of the model can be constrained. This suppresses the antisymmetric mode flutter because a roll degree of freedom makes it critical for this model.

Modal Characteristics

The flutter analysis requires natural vibration modes, which can be determined by a modal test and analysis. The modal test has been conducted using the dynamic displacement measurement system (DDMS) [20] developed by JAXA. The DDMS can automatically

Table 1 Modal characteristics in free-flight configuration

Mode	Natural frequency, Hz		Mode shape
	Test	Analysis	
0	——	——	Roll mode
1	63	65	Symmetric first bending
2	73	76	Antisymmetric first bending
3	91	89	Symmetric first torsion
4	91	89	Antisymmetric first torsion
5	131	142	Symmetric mode
6	133	144	Antisymmetric mode
7	196	185	Symmetric mode

measure the dynamic displacement with a laser vibrometer, which is positioned by an arm-type robot, whereas the model is excited by an electromagnetic shaker with a white noise signal. The natural vibration modes have been calculated from the measured dynamic displacement of 74 points (21 on each main wing and 16 on each tip-fin). The test result is shown in Table 1 along with the result of an FEM analysis performed by employing the Lanczos method.

A comparison between these results shows that the mode shapes of the analysis and test are in reasonable agreement over all modes. Their natural frequencies are in good agreement up to the third mode, whereas they differ slightly in the fourth mode and above. It is considered that this difference is due to the simplification of the FEM model, which comprises beam elements and concentrated mass. The difference in higher modes is acceptable because flutter generally occurs due to coupling in lower modes. However, for flutter calculations, it is preferable to use the natural frequencies of the test and the mode shapes of the analysis because it is difficult to measure the vibration modes accurately in the test.

Flutter Characteristics

The flutter experiment was conducted in the 2×2 m transonic wind tunnel of JAXA. The model and supporting system in the wind tunnel are shown in Fig. 5. The critical flutter speed was determined by increasing the total pressure in steps at certain Mach numbers. Flutter can be suppressed by the supporting system. Figure 6 shows the time histories of the strain of the wing at $M = 0.8$. The figures on the left show the time histories from the occurrence of flutter to its suppression. The figures on the right show magnified time histories that correspond to the occurrence of flutter. These histories reveal that the flutter modes are antisymmetric and they can be suppressed by the supporting system. Therefore, flutter points could be determined at Mach numbers 0.6, 0.8, 0.96, 1.1, and 1.2.

We now perform the flutter analysis. The DPM is employed to calculate unsteady aerodynamics. The antisymmetric and symmetric modes can be treated separately by the linear theory on which the DPM is based; this results in a reduction in computation time. The zeroth, second, fourth, and sixth modes are used to compute the antisymmetric mode flutter, whereas the first, third, fifth, and seventh modes are used to determine the symmetric mode flutter. The Mach numbers selected are 0.6, 0.7, 0.8, 0.96, 1.1, 1.2, 1.3, and 1.4. The aerodynamic panel for calculating the unsteady aerodynamics comprises 252 elements (120 for the main wing, 36 for the tip-fin, and 96 for the fuselage), as shown in Fig. 7. The flutter speeds are calculated by the p–k method [21] with a structural damping of 0.03. The antisymmetric mode flutter that is coupled with the second and fourth modes becomes critical in the analysis. The symmetric mode flutter that is coupled with the first and third modes is also calculated. In the free-flight configuration, the antisymmetric flutter becomes critical and its speed is less than that of the symmetric flutter. Figure 8 shows a plot of the experimental and analytical nondimensional flutter speeds. By assuming that the flow is inviscid, irrotational, and isentropic, the nondimensional flutter speed is defined by Eq. (1) [22].

$$\bar{U}_F = \frac{U_F}{b\omega_\alpha \sqrt{\mu}} \tag{1}$$

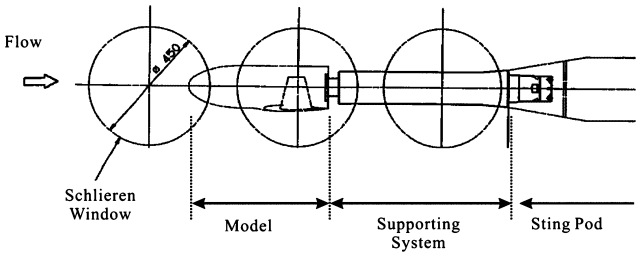

Fig. 5 Wind tunnel setting.

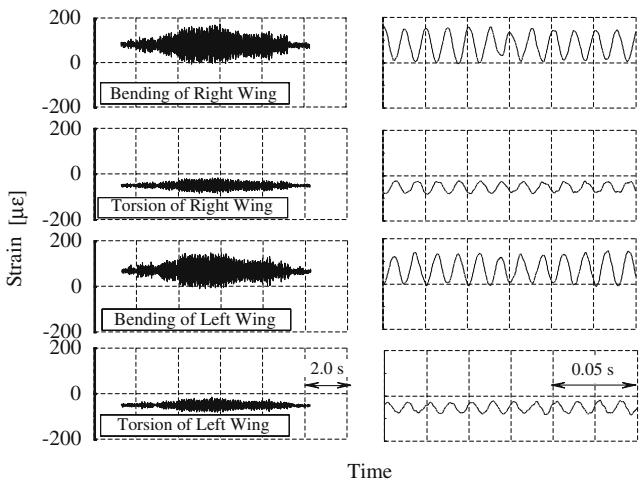

Fig. 6 Time histories of strain in free-flight configuration.

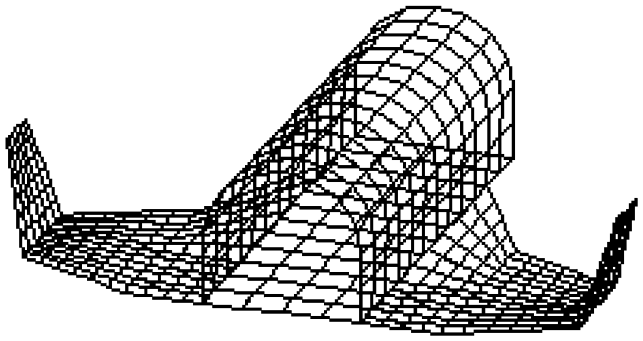

Fig. 7 Aerodynamic panel.

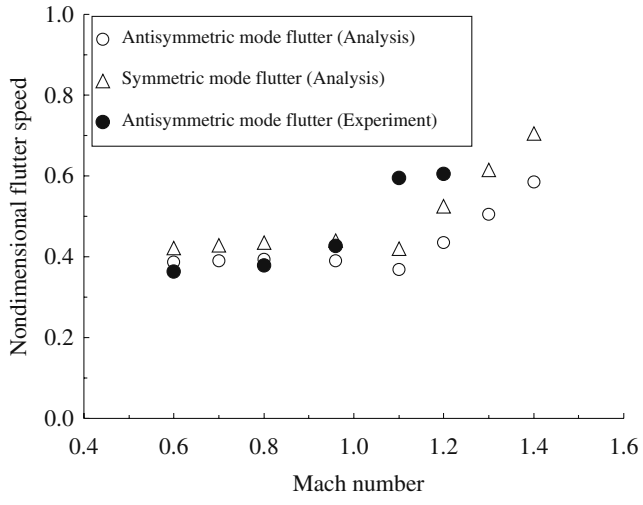

Fig. 8 Flutter speed in free-flight configuration.

Equation (1) can also be expressed in terms of M and P_0 as follows:

$$\bar{U}_F = \frac{1}{2\pi f_\alpha b}\sqrt{\frac{\pi b S_w}{2m}}\sqrt{\frac{\gamma P_0 M^2}{1+(\gamma-1)M^2/2}} \tag{2}$$

The analysis and experimental results are in good agreement except in the supersonic region.

Next, we consider the difference between the analytical and experimental flutter speeds in the supersonic region. At $M = 1.1$ and 1.2, the experimental flutter speeds are greater than the analytical ones. One interpretation of this discrepancy is that the Mach number used to calculate the unsteady aerodynamics may be different from the Mach number around the wing. The Mach number of the freestream has been used in the flutter analysis. It should be noted that the wings of the wind tunnel model are nonplanar and the area surrounded by the fuselage, main part of the wing, and tip-fin is narrow. This results in a channel flow around the wing. We attempt to resolve the discrepancy by performing flutter analysis with the measured local Mach number, as described later.

Flutter in Launching Configuration

This section describes the flutter characteristics of the reentry space vehicle model in the launching configuration. To simulate this configuration in the wind tunnel test, the supporting system developed for the free-flight configuration was remodeled and a roll elastic freedom was provided to the wind tunnel model. The flutter experiment was conducted in the transonic wind tunnel of JAXA, as in the case of the free-flight configuration. The flutter analysis was then conducted by employing the DPM and the result was compared with that of the experiment.

Wind Tunnel Model and Supporting System

The wind tunnel model in the launching configuration is shown in Fig. 9. With the exception of the wing structure, the shape of the model is the same as that in the free-flight configuration. The wind tunnel model for the free-flight configuration was damaged during the test; hence, the wing structure was changed by increasing the strength of the wing. Strain gauges were installed on the root of the wing for measuring the bending and torsion strain during the wind tunnel test.

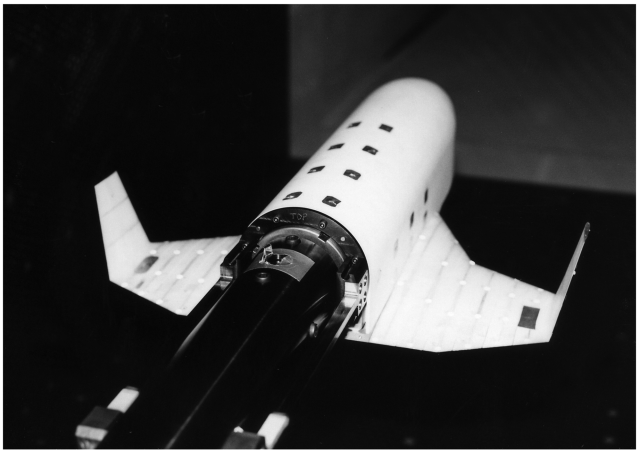

Fig. 9 Wind tunnel model for launching configuration.

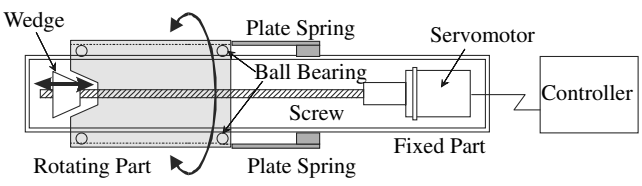

Fig. 10 Schematic of supporting system for launching configuration.

Table 2 Modal characteristics in launching configuration

Mode	Natural frequency, Hz		Mode shape
	Test	Analysis	
0	21	21	Roll mode
1	67	69	Symmetric first bending
2	81	82	Antisymmetric first bending
3	97	107	Symmetric first torsion
4	98	108	Antisymmetric first torsion
5	205	246	Symmetric second torsion
6	208	247	Antisymmetric second torsion
7	253	286	Symmetric mode

The original supporting system that allowed free rolling motion was remodeled to provide a roll elastic freedom to the model. The schematic of the supporting system is shown in Fig. 10. As shown in this figure, two plate springs, which provide the roll elastic freedom to the model, are attached to the right and left sides of the supporting system. A strain gauge is attached to observe the flutter on each plate spring. It should be noted that the supporting system can be restored to its original setting by removing the plate springs. The remodeled supporting system can also serve as a means of flutter suppression.

Modal Characteristics

The natural vibration modes determined by the analysis and test are listed in Table 2. A comparison between the results of the analysis and test reveals that the natural frequencies of the zeroth, first, and second modes are in good agreement. However, in the third mode and above, the natural frequencies of the analysis are greater than those of the test by 10–20%. This difference can be attributed to the simplification of the FEM model, which comprises the beam elements and concentrated mass. On the other hand, the mode shapes of the analysis and test are in reasonable agreement over all modes. It should be noted that the existence of the spring affects the mode shapes and frequencies of the zeroth and second modes. The difference between the natural frequencies of the symmetric modes listed in Tables 1 and 2 depends on the difference in the wing structure.

Flutter Characteristics

The flutter experiment was conducted in the transonic wind tunnel. The flutter points of the wind tunnel model with the spring were determined by increasing P_0 in steps at certain Mach numbers. Flutter was suppressed by the supporting system. Figure 11 shows the time histories of the strain of the wing at $M = 0.6$. The figures on the left show the time histories from the occurrence of flutter to its suppression. The figures on the right show magnified time histories that correspond to the occurrence of flutter. It should be noted that the strain outputs of the amplifier were saturated during the occurrence of flutter. Based on the histories, we inferred that the antisymmetric mode flutter occurred and it could be suppressed by the remodeled supporting system. The flutter points were determined at Mach numbers 0.6, 0.7, 0.8, 0.96, and 1.2.

The flutter speeds are calculated by the DPM and p–k method. The zeroth, second, fourth, and sixth modes are used to compute the antisymmetric mode flutter, whereas the first, third, fifth, and seventh modes are used to determine the symmetric mode flutter. The Mach numbers selected are 0.6, 0.7, 0.8, 0.96, 1.2, and 1.4. The aerodynamic panel of the right wing comprises 196 elements (60 for the main wing, 36 for the tip-fin, and 100 for the fuselage). The flutter analysis is performed by using the natural frequencies of the test and the mode shapes of the FEM analysis. The result reveals that the antisymmetric mode flutter that is coupled with the second and fourth modes becomes critical. A symmetric mode flutter that is coupled with the first and third modes is also estimated. The analytical and experimental flutter speeds are shown in Fig. 12a; they are in good agreement except in the supersonic region. It is found that the speed of the antisymmetric mode flutter is less than that of the symmetric mode flutter, as in the case of the free-flight configuration.

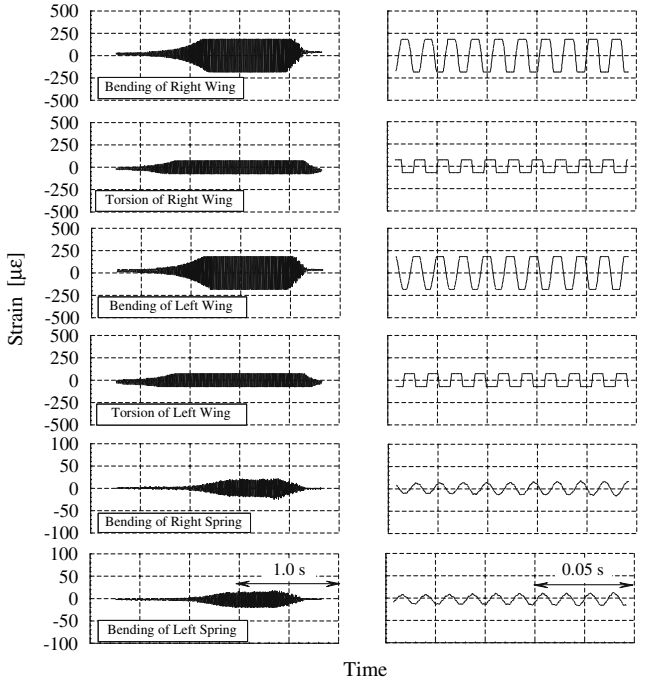

Fig. 11 Time histories of strain in launching configuration.

Next, we examine the antisymmetric mode flutter in greater detail. A strong spring, whose rigidity is greater than that of the nominal spring, is used to examine the effect of the rigidity of the roll spring on flutter. In the presence of the strong spring, the natural frequencies of the zeroth and second modes of the model become 40 Hz and 87 Hz, respectively, (21 Hz and 82 Hz for the nominal spring, as listed in Table 2). Antisymmetric mode flutter analyses have been performed with and without the nominal and strong springs. Figure 12b shows the speed of the antisymmetric mode flutter. It should be noted that high roll stiffness decreases the speed of the antisymmetric flutter due to variations in the second natural vibration mode (the antisymmetric first bending mode). The variations occur because the roll stiffness remarkably changes the characteristics of the natural vibration mode.

The analytical and experimental flutter speeds differ significantly at $M = 1.2$; the experimental flutter speed is greater than the analytical one. This result is also obtained in the case of the free-flight configuration. It is anticipated that the difference between the Mach number of the local flow around the wing and that of the freestream results in the discrepancy in the flutter speeds because of the nonplanar wings and blunt fuselage. We attempt to resolve this discrepancy by performing the flutter analysis with the measured local Mach number, as described in the following section.

Flutter Boundary Correction

In the free-flight configuration, the experimental flutter speed is significantly greater than the analytical one at $M = 1.1$ and 1.2. A similar result is obtained at $M = 1.2$ in the launching configuration. It is evident from these results that the supersonic region requires further consideration. It is anticipated that the Mach number of the local flow around the wing, which differs from the freestream, causes a difference in the flutter speeds. In this section, static and dynamic pressures around the wing are measured to determine the local Mach number in the channel flow. We attempt to explain the discrepancy by performing the flutter analysis with local Mach numbers.

Pressure Measurement

A rigid wind tunnel model was developed for measuring the static and total pressures of the local flow. The shape of the rigid model is the same as that of the models used in previous flutter experiments. The static pressure P_1 is measured using four pressure sensors installed in the main part of the right wing. Two sensors are located at

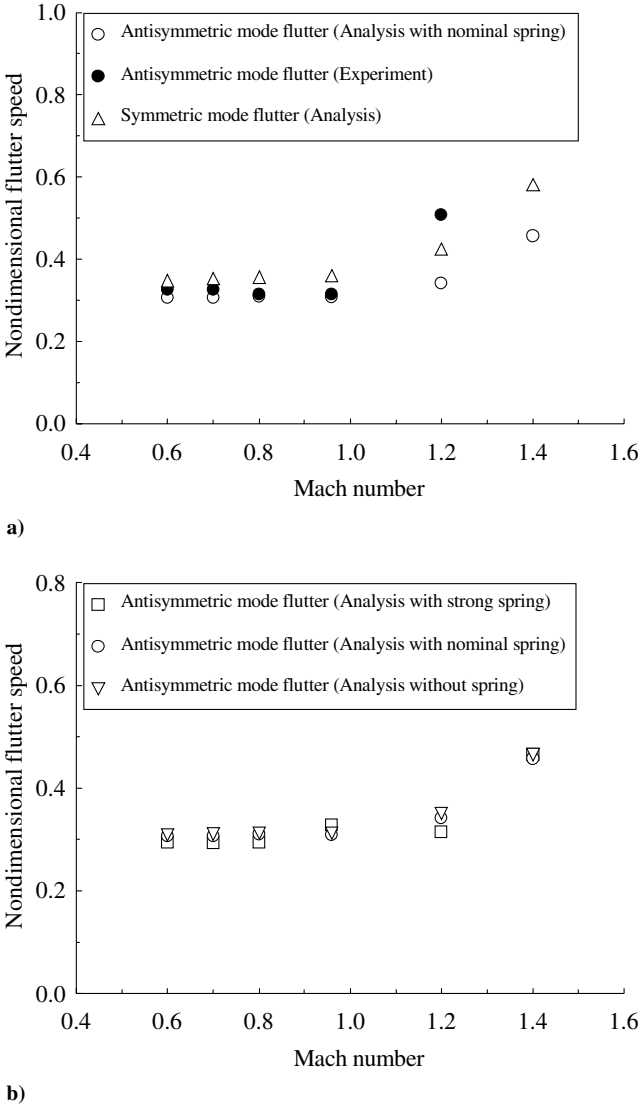

Fig. 12 a) Flutter speed in launching configuration; b) antisymmetric mode flutter in launching configuration.

chords of 31.1 and 90.7% on the span 45.5 mm inboard, and the other two are located at chords of 31.1 and 81.5% on the span 140.5 mm outboard.

The total pressure around the wing is measured using two Pitot tubes, which can be moved manually along the axis of the wind tunnel model. The Pitot tubes are installed on the left wing to avoid interaction with the pressure sensors on the right wing. The spanwise positions of the Pitot tubes are collocated to the positions of the pressure sensors. The wind tunnel model with the Pitot tubes and pressure sensors is shown in Fig. 13. The model in the wind tunnel is shown in Fig. 14. The total and static pressures are measured under a steady flow condition with Mach numbers 0.6, 0.8, 1.0, 1.1, 1.2, 1.3, and 1.4. The values of P_0 in a plenum chamber are 80 and 100 kPa.

Local Mach Nnumber

As shown in Fig. 15, the total pressure is measured as P_{02}, which is generated behind a shock wave produced by the Pitot tubes in the supersonic region. The relationship between the local Mach number M_1, P_1, and P_{02} is given by Eq. (3), which is known as the Rayleigh Pitot tube formula [23].

$$\frac{P_1}{P_{02}} = \frac{P_1}{P_2}\frac{P_2}{P_{02}} = \left(\frac{2\gamma}{\gamma+1}M_1^2 - \frac{\gamma-1}{\gamma+1}\right)^{1/\gamma-1}\left(\frac{\gamma+1}{2}M_1^2\right)^{\gamma/1-\gamma} \tag{3}$$

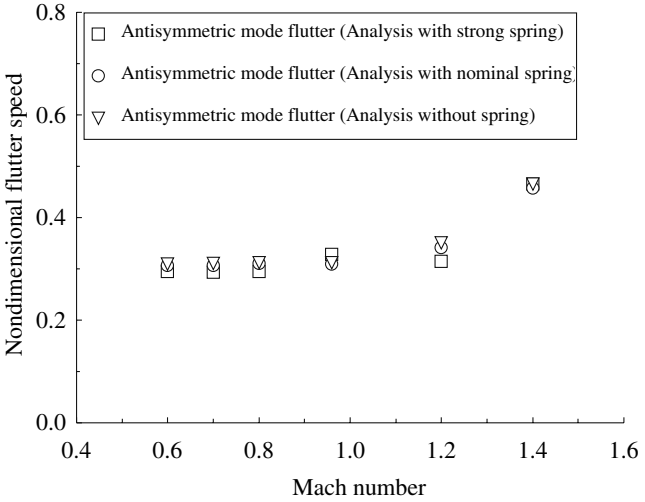

Fig. 13 Pitot tubes and pressure sensors.

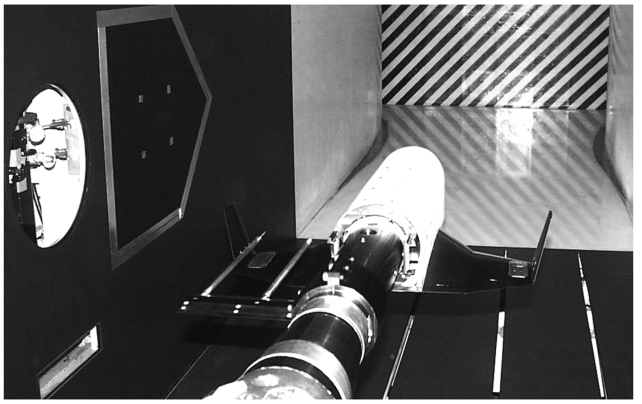

Fig. 14 Wind tunnel model for pressure measurement.

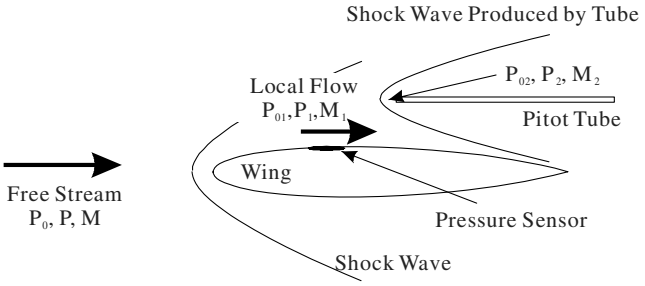

Fig. 15 Flow around wing.

M_1 is calculated by the regula falsi method using the measured values of P_1 and P_{02} in the supersonic region. On the other hand, the local Mach number for the subsonic region is calculated using Eq. (4).

$$\frac{P_1}{P_0} = \left[1 + \frac{(\gamma - 1)M_1^2}{2}\right]^{\gamma/1-\gamma} \tag{4}$$

The distributed local Mach numbers are determined at each pressure sensor. A typical flutter analysis based on the lifting surface theory requires a representative Mach number. The simplest method for estimating the representative Mach number is to calculate the average value of M_1. The critical flutter is the coupling of the second and fourth natural vibration modes. In these modes, the deflection in the outboard wing is greater than that in the inboard wing. The outboard local flow has a greater effect on the unsteady aerodynamics. Therefore, this study uses the average value of M_1 (corrected Mach number) determined only for the outboard as the

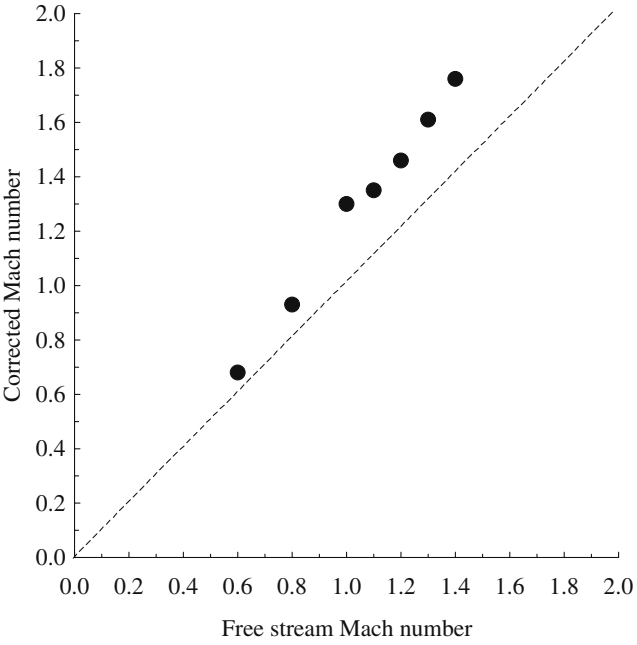

Fig. 16 Corrected Mach number.

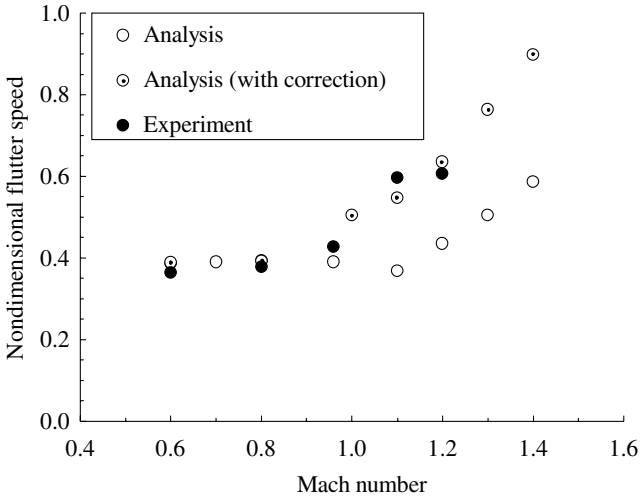

a)

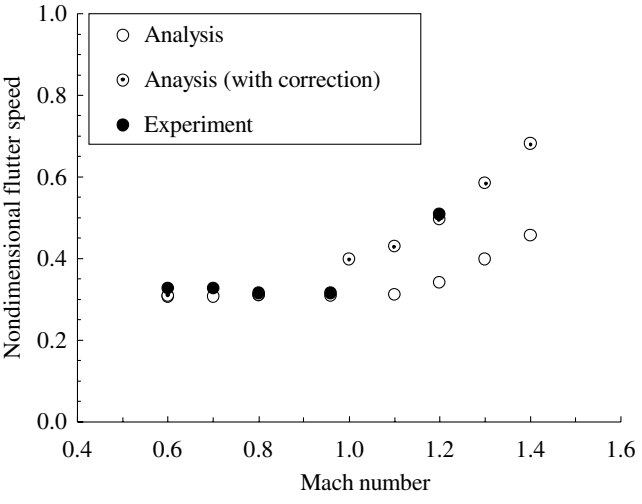

b)

Fig. 17 a) Corrected flutter speed in free-flight configuration; b) corrected flutter speed in launching configuration.

representative Mach number. The corrected Mach number obtained by the experiment is shown in Fig. 16. It is found that the corrected Mach numbers are significantly greater than the freestream Mach numbers.

Flutter Boundary Correction

The flutter analysis is performed by using M' instead of the freestream Mach number. The corrected flutter speeds are shown in Figs. 17a and 17b for the free-flight and launching configurations, respectively. It should be noted that the flutter speeds in the local stream are corrected. They must be converted into flutter speeds in the freestream. However, the exact difference between the local and freestreams is unknown. On the other hand, based on an analogy with an experiment conducted under the near stream condition, it is found that the flutter speed in the freestream at Mach number 1.2 is less than that in the local stream by only 1%. In a low supersonic region, the difference between the flutter speeds of the local and freestreams is not very large and can be neglected. The corrected and experimental flutter speeds are in good agreement. It can be concluded that the difference between the Mach numbers of the freestream and local flow results in the discrepancy in the flutter speed. The Mach number of the local flow must be considered for the flutter analysis of nonplanar wings such as those of HOPE.

The correction of the analysis is not limited to the supersonic region. The result indicates that the correction has little influence on the flutter speed in the subsonic and transonic regions. One reason is that the difference between the Mach numbers in the subsonic and transonic regions is less than that in the supersonic region (see Fig. 16). Another reason is that in the subsonic region, the dependence of the flutter speed on the Mach number is rather small.

Conclusions

Flutter analyses of the reentry space vehicle that has a roll elastic body-freedom have been performed by employing the doublet-point method. The result reveals that the flutter that is coupled with the antisymmetric first bending and the antisymmetric first torsion modes of the wing becomes critical like in the free-flight configuration (without a roll elastic body-freedom). It is also shown that the existence of the roll elastic body-freedom further decreases the critical flutter speed. This phenomenon is caused by variations of the characteristics of the antisymmetric first bending modes of the wing due to the roll stiffness.

In the supersonic region, the experimental flutter speed is significantly greater than the analytical one. The analytical result by using the measured local Mach number instead of the Mach number of the uniform flow indicates that the corrected and experimental flutter speeds are in good agreement. It is concluded that the interference between the nonplanar wings and blunt fuselage changes the flow parameters for the unsteady aerodynamic calculations in the supersonic region.

References

[1] Yamanaka, T., "Overview of Japanese Aerospace Plane," AIAA Paper 92-5005, Dec. 1992.

[2] Ito, T., Akimoto, T., Miyabe, H., Kano, Y., Suzuki, N., and Sasaki, H., "Concept and Technology Development for HOPE Spaceplane," AIAA Paper 90-5223, Oct. 1990.

[3] Dugundji, J., "Personal Perspective of Aeroelasticity During the Years 1953–1993," *Journal of Aircraft*, Vol. 40, No. 5, 2003, pp. 809–812.

[4] Livne, E., and Weisshaar, T. A., "Aeroelasticity of Nonconventional Airplane Configurations-Past and Future," *Journal of Aircraft*, Vol. 40, No. 6, 2003, pp. 1047–1065.

[5] Niblett, L. T., "The Fundamentals of Body-Freedom Flutter," *Aeronautical Journal*, Vol. 90, Nov. 1986, pp. 373–377.

[6] Weisshaar, T. A., and Crittenden, J. B., "Flutter of Asymmetrically Swept Wings," *AIAA Journal*, Vol. 14, No. 8, 1976, pp. 993–994.

[7] Miller, G. D., Wykes, J. H., and Brosnan, M. J., "Rigid-Body Structural Mode Coupling on a Forward Swept Wing Aircraft," *Journal of Aircraft*, Vol. 20, No. 8, 1983, pp. 696–702.

[8] Weisshaar, T. A., and Zeiler T. A., "Dynamic Stability of Flexible Forward Swept Wing Aircraft," *Journal of Aircraft*, Vol. 20, No. 12, 1983, pp. 1014–1020.

[9] Chipman, R., Rauch, F., Rimer, M., Muniz, B., and Ricketts, R. H., "Transonic Tests of a Forward Swept Wing Configuration Exhibiting Body Freedom Flutter," AIAA Paper 85-0689, Apr. 1985.

[10] Banerjee, J. R., "Flutter Characteristics of High Aspect Ratio Tailless Aircraft," *Journal of Aircraft*, Vol. 21, No. 9, 1984, pp. 733–736.

[11] Chen, G. S., and Dugundji, J., "Experimental Aeroelastic Behavior of Forward-Swept Graphite/Epoxy Wings with Rigid-Body Freedom," *Journal of Aircraft*, Vol. 24, No. 7, 1987, pp. 454–462.

[12] Soistmann, D. L., and Spain, C. V., "An Experimental and Analytical Study of a Lifting-Body Wind-Tunnel Model Exhibiting Body-Freedom Flutter," AIAA Paper 93-1316, Apr. 1993.

[13] Wu, Z., and Yang, C., "Flight Loads and Dynamics of Flexible Air Vehicles," *Chinese Journal of Aeronautics*, Vol. 17, No. 1, 2004, pp. 17–22.

[14] Wykes, J. H., and Lawrence, R. E., "Aerothermoelasticity: Its Impact on Stability and Control of Winged Aerospace Vehicles," *Journal of Aircraft*, Vol. 2, No. 6, 1965, pp. 517–526.

[15] Kobayashi, S., Isono, K., Wasiya, M., Kakizaki, S., and Ueda, T., "Low Speed Wind Tunnel Experiment for Body Flutter," *Journal of the Japan Society for Aeronautical and Space Sciences*, Vol. 45, No. 517, 1997, pp. 86–92.

[16] Kanda, A., and Ueda, T., "Wind Tunnel Tests and Analysis on Flutter of Spacecraft Including Pitching Effects in Its Launching Configuration," *Proceedings of International Forum on Aeroelasticity and Structural Dynamics*, NASA Langley Research Center, Hampton, VA, 1999, pp. 115–120.

[17] Kanda, A., and Ueda, T., "Flutter Characteristics of Winged Vehicle in Free-Flight/Launching Configuration and Development of Model Supporting System," *Journal of the Japan Society for Aeronautical and Space Sciences*, Vol. 49, No. 573, 2001, pp. 346–353.

[18] Kanda, A., "Wind Tunnel Test and Analysis of Yawing Mode Flutter of Japanese Reentry Space Vehicle HOPE with Nonplanar Wing," *Proceedings of International Forum on Aeroelasticity and Structural Dynamics* [CD-ROM], Netherlands Association of Aeronautical Engineers, Amsterdam, 2003.

[19] Ueda, T., "Unsteady Aerodynamic Calculations for General Configurations by the Doublet-Point Method," National Aerospace Laboratory of Japan, TR-1101T, Tokyo, 1991.

[20] Sotozaki, T., and Ueda, T., "Preliminary Vibration Tests Using the Dynamic Displacement Measurement System," National Aerospace Laboratory of Japan, TM-683, Tokyo, 1995.

[21] Hassig, H. J., "An Approximate True Damping Solution of the Flutter Equation by Determinant Iteration," *Journal of Aircraft*, Vol. 8, No. 11, 1971, pp. 885–889.

[22] Bisplinghoff, R. L., and Ashley, H., *Principle of Aeroelasticity*, Dover, New York, 2002, pp. 235–258.

[23] Anderson, J. D., *Fundamentals of Aerodynamics*, 2nd ed., McGraw–Hill, New York, 1991, pp. 448–452.

B. Balachandran
Associate Editor